

## PREFERRED ORIENTATION PATTERNS OF PHYLLOSILICATES IN SURFACE CLAYS

H.-R. WENK<sup>1</sup> AND R. VASIN<sup>1,2</sup>

<sup>1</sup> Department of Earth and Planetary Science, University of California, Berkeley, California, USA

<sup>2</sup> Joint Institute for Nuclear Research, Dubna, Moscow Region, Russia

**Abstract**—The alignment of phyllosilicates in clays has received a lot of attention because it is a major cause of seismic anisotropy in the Earth's crust. Thus far, all attention has been on shales where the orientation pattern has been attributed to compaction and observed to increase with burial depth and diagenetic processes. Here, for the first time, the same methods that were developed to quantify shale preferred orientation were applied to clays forming in surface environments, a seasonal streambed in Death Valley, California; a mudpool from mud volcanoes in Imperial Valley, California, close to the Salton Sea; and a glacial lake from Val Albigna in the Swiss Alps. Preferred orientation was analyzed quantitatively with high-energy synchrotron X-ray diffraction. All three samples showed strong alignment of phyllosilicates with (001) pole figure maxima 2–4 multiples of a random distribution, comparable to shales, and indicating that significant preferred orientation can be produced at surface conditions. The original alignment during sedimentation may be an important factor for the final microstructure in many shales.

**Key Words**—Albigna Glacial Lake, Clay Fabric, Death Valley, Preferred Orientation, Salton Sea Mud Volcanoes, Surface Clays, Synchrotron X-rays.

### INTRODUCTION

Phyllosilicate-rich sediments and sedimentary rocks are generally highly anisotropic. Much attention has been given to them as capstones of oil and gas reservoirs and as seals in the context of nuclear waste repositories and carbon dioxide storage (*e.g.* Chadwick *et al.*, 2004; Aplin and Larter, 2005; Bossart and Thury, 2007; Almquist and Mainprice, 2017). The anisotropy of physical properties, such as acoustic wave velocities, is due to the alignment of platelet-shaped phyllosilicate crystals and pores. This preferred orientation (also referred to as fabric or texture) in shales is thought to increase with burial depth and compaction (*e.g.* Aplin *et al.*, 2006), diagenesis (*e.g.* Ho *et al.*, 1999), and phyllosilicate content (*e.g.* Curtis *et al.*, 1980) and is used in rock-physics models to predict elastic anisotropy (*e.g.* Ruud *et al.*, 2003; Dræge *et al.*, 2006). Orientation patterns are moderate in shales, with platelets aligning in the bedding plane and concentrating 2–10 times compared to a random pattern (multiples of random distribution or m.r.d.). In recrystallized metamorphic slates, schists, and gneisses, orientations can be stronger with concentrations reaching 20–50 m.r.d. (*e.g.* Wenk *et al.*, 2010; Haerincx *et al.*, 2015).

The purpose of the present study was to quantify for the first time the phyllosilicate orientation patterns in clays forming at surface conditions by investigating

three different types of clay-rich environments, namely, dried surface-mud deposits from a seasonal stream in Death Valley, California, clay from mud volcanoes in Imperial Valley, California, and mud from a glacial lake deposit in the Swiss Alps, using hard synchrotron X-rays to record diffraction images and to quantify preferred orientation patterns with a modified Rietveld method (Lutterotti *et al.*, 2014).

### SAMPLES AND EXPERIMENTS

The first sample, DV1, was collected in a dry seasonal stream bed East of Stovepipe Wells, Death Valley National Park, California, between highway 190 and the Mesquite Flat sand dunes (Figure 1a, coord. 36°36'21"N/117°6'58"W). On the outcrop, the clay formation is dry and exhibits typical hexagonal desiccation cracks. The second sample, SS2, is a brownish clay from an outcrop near the Davis and Schrimpf road intersection in Niland, Imperial Valley, California, near the Salton Sea (coord. 33°11'55"N/115° 34'46"W) and is part of mud volcanoes that are currently active (*e.g.* Helgeson, 1968; Sturz, 1989; Rudolph and Manga, 2010) (Figure 1b). The sample used in the present study was collected from a dry site, again characterized by mud cracks. The third sample, Brg1644, is from a small glacial lake in Val Albigna, southeastern Switzerland (coord. 46°19'31"N/9°38'57"E), between the end of the glacier and a large reservoir used for hydroelectric power (Figure 1c).

The microstructure was first explored with scanning electron microscopy (SEM), using a Zeiss Evo MA10 SEM instrument (Oberkochen, Germany), equipped with

\* E-mail address of corresponding author:

wenk@berkeley.edu

DOI: 10.1346/CCMN.2017.064069

an EDAX energy-dispersive spectroscopy (EDS) system at UC Berkeley, and a JEOL SEM (JEOL IT 300, Akishima, Japan), at the Engineering Faculty of the University of Trento in Mesiano, Italy. For the SEM study, broken fragments of the clay samples were coated

with carbon to prevent charging. At both facilities, samples were analyzed in high-vacuum mode. In electron backscatter images (Figure 2), bright shades are indicative of high atomic numbers. Elemental compositions of Death Valley clay and Salton Sea clay were established by EDS spectroscopy, averaging over an area  $1\text{ mm} \times 1\text{ mm}$  (Figure 3).

The hard X-ray synchrotron diffraction measurements were performed at beamline BESSRC 11-ID-C of the Advanced Photon Source at Argonne National Laboratory (see Wenk *et al.*, 2010 for details of the

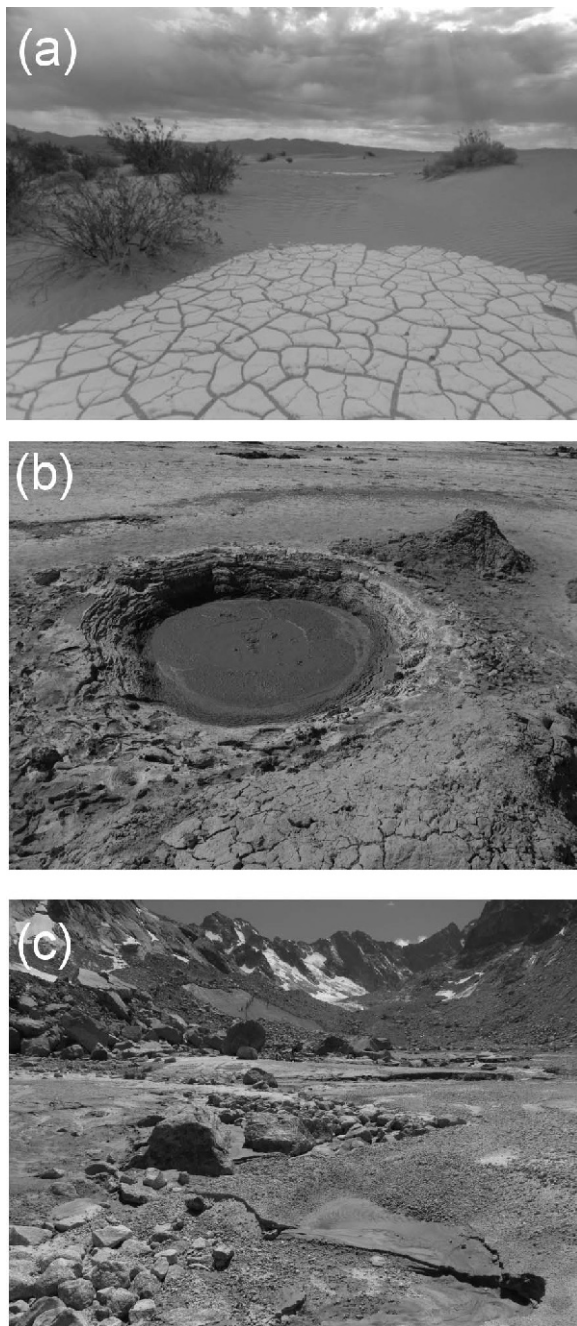


Figure 1. Outcrop pictures. (a) Death Valley, California, USA, near Mesquite Flat sand dunes. Notice hexagonal pattern of drying cracks (courtesy of Instagram@ExtremeNature). (b) Mud volcano in Imperial Valley, California, USA, near Salton Sea. (c) Val Albigna, Swiss Alps with a mud pond in the foreground and the glacier in the back.

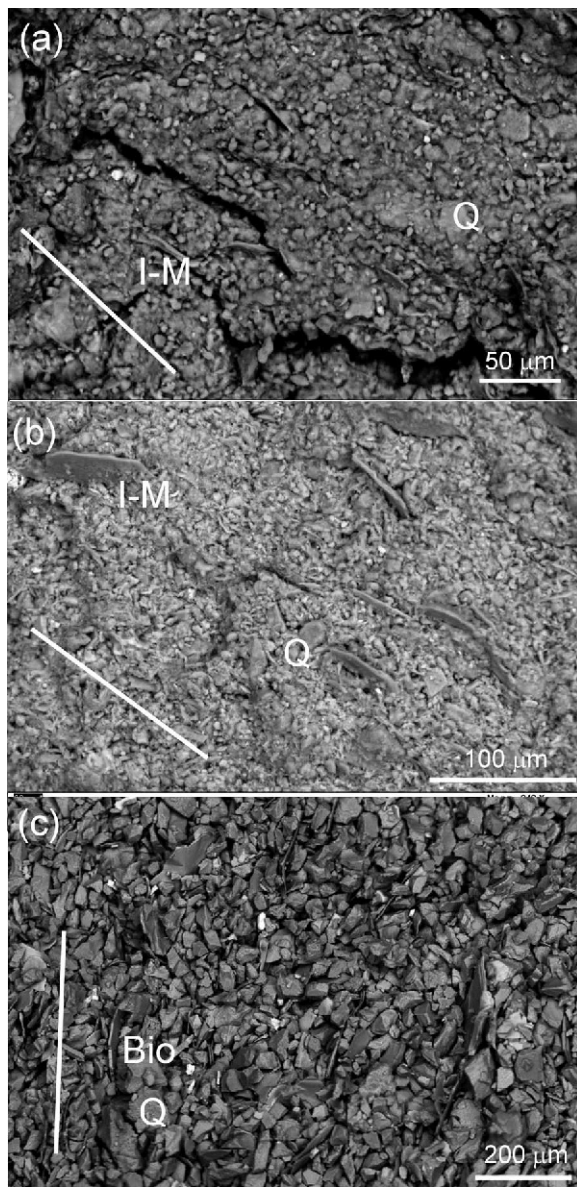


Figure 2. SEM backscattered images of microstructures: (a) Death Valley, (b) Salton Sea mud volcano, and (c) Val Albigna glacial pond. For mineral abbreviations see Table 1. The white line indicates the bedding plane.

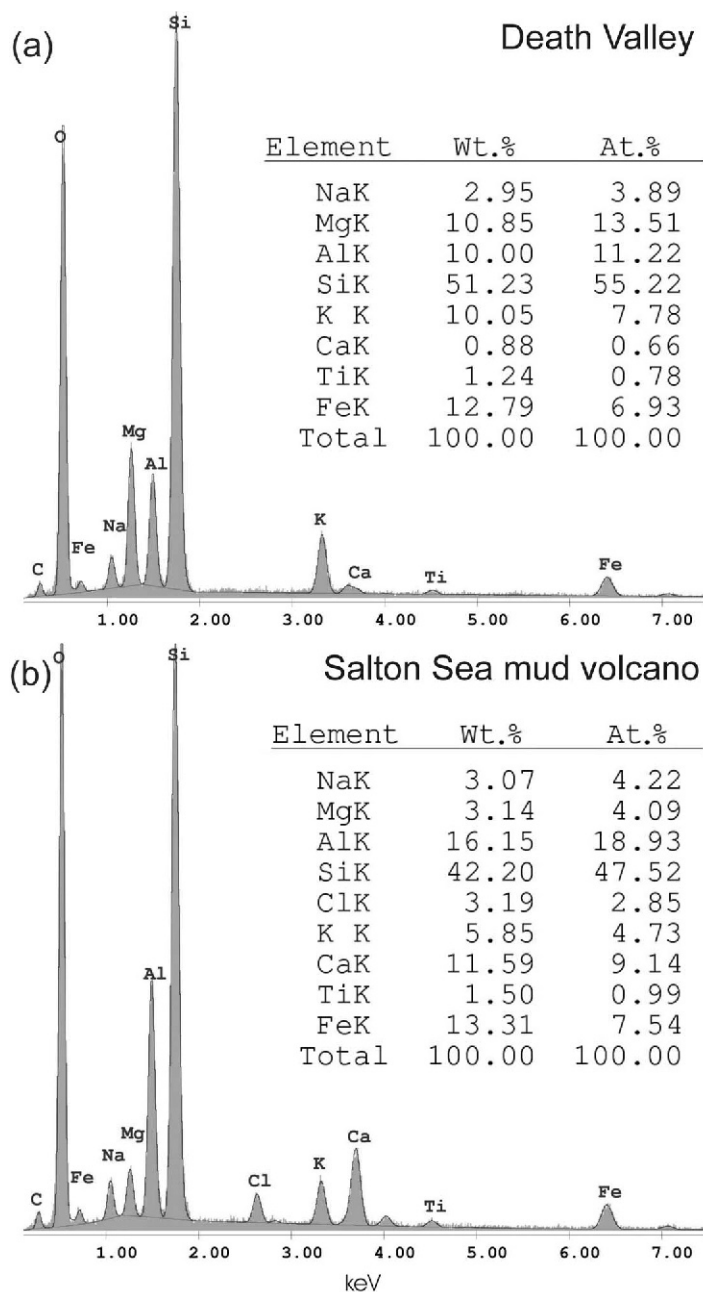


Figure 3. SEM-EDS spectra of (a) Death Valley and (b) Salton Sea clays and normalized estimated atomic composition of major elements, excluding O. Scale is energy (keV).

texture measurements). A monochromatic X-ray beam with a wavelength  $\lambda = 0.10798 \text{ \AA}$  and a beam diameter of 1 mm was used for the investigation of samples DV1 and SS2, while a wavelength of  $0.117418 \text{ \AA}$  was used to record diffraction patterns of the Brg1644 sample. To ensure a uniform system for graphic representations of diffraction patterns, a scattering vector magnitude  $q = 2\pi/d = (4\pi \sin\theta/\lambda)$  was used for the horizontal axis rather than the scattering angle  $2\theta$ . Diffraction images were recorded with a Perkin Elmer 1621 amorphous

silicon detector (2048 pixels  $\times$  2048 pixels) (Perkin Elmer, Waltham, Massachusetts, USA), at a distance of  $\sim 200 \text{ cm}$  from the sample. For DV1 and SS2, the samples were slabs 2 mm thick and analyzed dry, as collected in the field. Sample Brg1644 was formed into a cylinder,  $\sim 3 \text{ mm}$  in diameter, extracting it with a kapton tube, and was analyzed wet. The samples were mounted on a goniometer with the axis perpendicular to the incident beam and aligned with the rotation axis centered on the beam and perpendicular to it

( $\pm 0.1$  mm) and then rotated in  $15^\circ$  increments around the normal to the bedding plane from  $-45^\circ$  to  $+45^\circ$  (slabs of DV1 and SS2), and from  $-90^\circ$  to  $+75^\circ$  (cylinder of Brg1644). The rotations were necessary to obtain adequate pole figure coverage to determine preferred orientation. At each rotation position, diffraction images (Figure 4) were recorded while the sample was translated 2 mm parallel to the rotation axis to obtain a representative volume average over  $\sim 6$  mm<sup>3</sup>.

Mineralogical compositions and preferred orientations were obtained by applying a modified Rietveld refinement (Rietveld, 1969) implemented in the software *MAUD* (for details and a step-by-step tutorial see Lutterotti *et al.*, 2014, and Wenk *et al.*, 2014). The Rietveld method obtains a best fit between measured diffraction patterns and a model based on a number of refined parameters, such as instrument geometry and resolution, background approximated by a polynomial

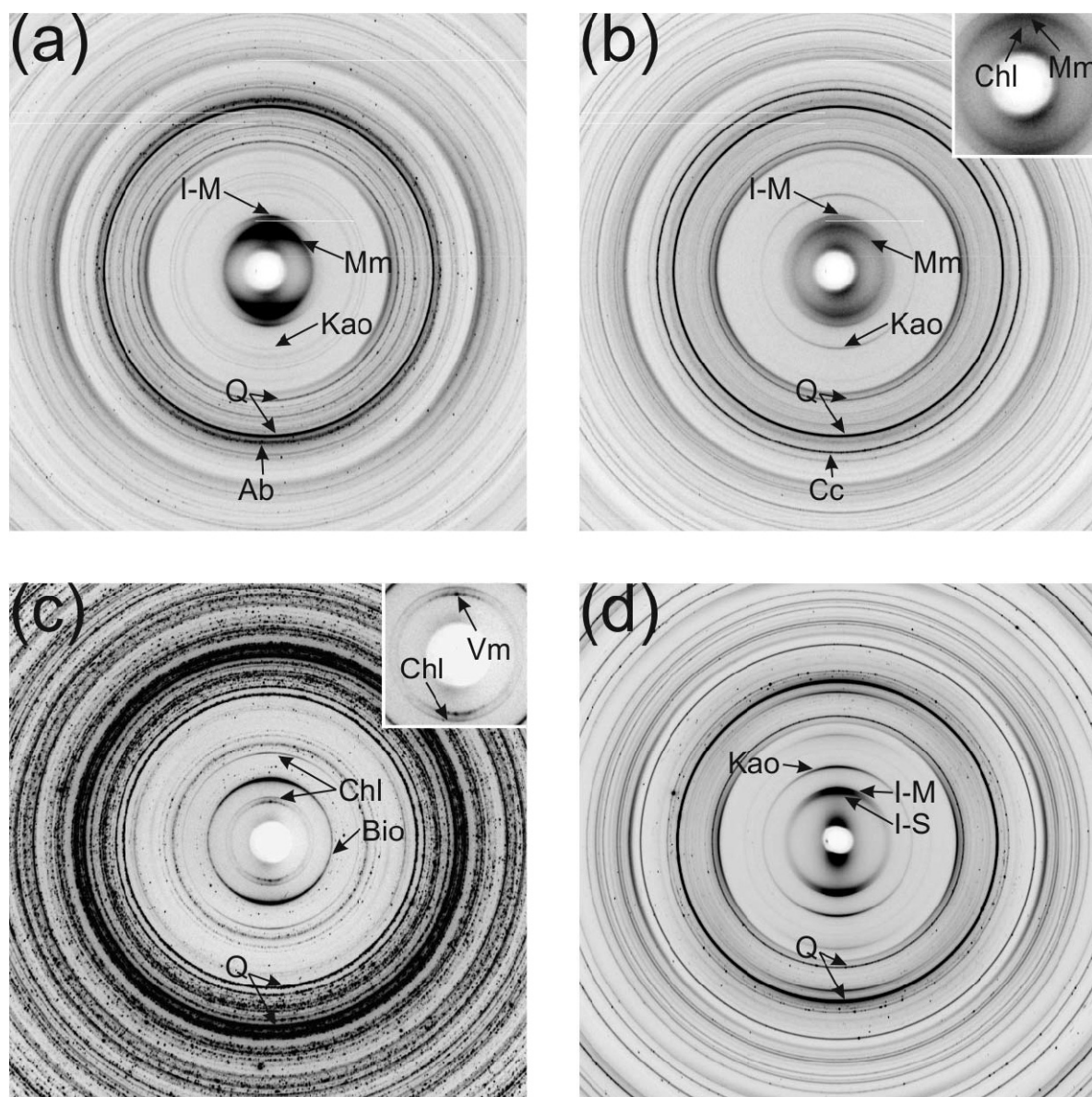


Figure 4. Synchrotron diffraction images comparing three surface clays: (a) Death Valley DV1; (b) Salton Sea mud volcano SS2; and (c) Val Albigna glacial lake Brg1644; with (d) Kimmeridge shale (Vasin *et al.*, 2013). Some Debye rings of phyllosilicates showing intensity variations along azimuthal angle expressing crystallite preferred orientation are marked: I-M (illite-mica), Mm (montmorillonite), Kao (kaolinite), Chl (chlorite), Bio (biotite), Vm (vermiculite), I-S (illite-smectite). Intensive peaks of several randomly oriented minerals, such as quartz (Q), calcite (Cc), and albite (Ab) are also indicated. Inserts show enlarged low-angle regions of corresponding diffraction images with overlapped phyllosilicate peaks. All images are rotated so that the bedding plane is horizontal. Note that image (c) was measured with a slightly different wavelength.

function, phase volume fractions, unit-cell parameters, crystal structure, preferred orientations, grain size, *etc.* First, instrument geometry was established by refining a diffraction image from a LaB<sub>6</sub> standard. Then diffraction images, measured at different sample tilts, were used to refine structure and microstructure parameters and determine preferred orientation of the phyllosilicates in the clay samples. Images were integrated over 10° azimuthal sectors in the *ImageJ* (Schneider *et al.*, 2012) *MAUD* plugin to obtain 36 conventional diffraction patterns at different azimuthal angles (a stack is shown in Figure 5, lower). This produced a total of  $7 \times 36 = 252$  diffraction patterns for DV1 and SS2 and  $12 \times 36 = 432$  patterns for Brg1644, and all patterns of each sample were refined simultaneously. For the Rietveld analysis, a scattering angle range from 0.28° to 3.52° was applied (corresponding to  $q$  values of 0.3–3.2 Å<sup>-1</sup>).

After the examination of SEM and diffraction images, seven mineral phases were considered for the DV1 refinement: montmorillonite, illite-muscovite, kaolinite, albite, orthoclase, quartz, and analcime; for the SS2 sample, ten components were used (montmorillonite, illite-muscovite, kaolinite, albite, chlorite, orthoclase, quartz, calcite, dolomite and pyrite); for Brg1644, seven components were used (biotite, vermiculite, chlorite, oligoclase, orthoclase, quartz, and hornblende).

The crystallographic information entered into *MAUD* as .cif files was from the literature: montmorillonite (Gournis *et al.*, 2008; amcsd #0009126), kaolinite (Bish and Von Dreele, 1989; amcsd #0012232), clinocllore/chlorite (Zanazzi *et al.*, 2009; amcsd #0007298), illite-muscovite (Gualtieri, 2000; amcsd #0012865), biotite (Brigatti and Davoli, 1990; amcsd #0001298), vermiculite (de la Calle *et al.*, 1977; amcsd # 0012759), quartz (Antao *et al.*, 2008; amcsd #0006212), albite (Downs *et al.*, 1994; amcsd #0001683), oligoclase An28 (Phillips *et al.*, 1971; amcsd #0010722), orthoclase (Tseng *et al.*, 1995; amcsd #0007928), calcite (Markgraf and Reeder, 1985; amcsd #0000984), dolomite (Ross and Reeder, 1992; amcsd #0001453), hornblende (Mancini *et al.*, 1996; amcsd #0005506), pyrite (Rieder *et al.*, 2007; amcsd #0012728), and analcime (Gatta *et al.*, 2006; amcsd #0004134).

In addition to mineral-volume fractions, relevant unit-cell and microstructure parameters of minerals were also refined, while atomic position coordinates and occupancies were kept fixed. Due to the complexity of diffraction patterns, no attempt was made to refine all crystallographic parameters, nor to impose anisotropic crystallite shapes for phyllosilicates.

The montmorillonite structure in DV1 and SS2 showed characteristic diffraction-peak broadening caused by stacking disorder. This factor was taken into account with the Ufer *et al.* (2004) method implemented in *MAUD* as the “Ufer single layer” model (Lutterotti *et al.*, 2010).

Intensity variations along some Debye rings (Figure 4) indicated immediately preferred orientation of clay minerals, *e.g.* montmorillonite (Mm) and illite-mica (I-M); by contrast, rings, *e.g.* for quartz (Q) and calcite (Cc), had uniform intensity. For comparison, a diffraction image (Figure 4d) of a typical sedimentary shale was added: Kimmeridge shale (Hornby, 1998; Vasin *et al.*, 2013). In Kimmeridge shale from considerable depth (>3000 m) the montmorillonite (peak at low angles, most notable in Death Valley clay) is missing. Qualitatively, intensity variations of phyllosilicate Debye rings of Kimmeridge shale are comparable to Death Valley clay.

Only phyllosilicates display significant preferred orientation and feldspars, quartz, and other minerals were considered to be randomly oriented. The E-WIMV model (Matthies and Vinel, 1982; Matthies, 2002), with a 10° resolution in orientation space, was used to refine phyllosilicate orientation distribution functions (ODF), without imposing axial symmetry around the bedding-plane normal. The 3D ODFs were exported from *MAUD* in a standard 5° × 5° × 5° grid, and smoothed with a 7.5° Gaussian filter in the *BEARTEX* software (Wenk *et al.*, 1998). The ODF was rotated to bring the bedding plane normal into the center of pole figures and corresponding pole figures were plotted in equal area projection. In all the texture-related calculations, the first setting for monoclinic crystals was used, as prescribed by E-WIMV algorithm rules, *i.e.* (100) is the cleavage plane of illite-muscovite, instead of the more familiar second setting with (001) as the cleavage plane (Matthies and Wenk, 2009). For labels of Miller indices (*hkl*) throughout this paper, the conventional second setting is used for monoclinic crystals, with (001) as the cleavage plane.

A polynomial function with five coefficients was applied to refine the background of each diffraction pattern. Broad intense peaks are visible on patterns of DV1 and SS2 samples at scattering angles  $2\theta < 0.5^\circ$  ( $d > 12.5$  Å) (Figures 4, 5) that are partially blocked by the beamstop. They can be interpreted as small-angle scattering from thin oriented montmorillonite and illite-mica platelets. In the refinement they were considered as additional background peaks in the same manner as for Kimmeridge shale (Wenk *et al.*, 2014).

The complexities of the diffraction pattern are most clearly visible in an average diffraction pattern over 36 individual patterns with different azimuths (Figure 6). Many diffraction peaks were contributed by the constituent phases (ticks below). The dot pattern is the measurement and the line is the Rietveld fit. The quality of the refinement can be assessed by comparing measured and calculated diffraction patterns (Figures 5, lower and upper, and 6). The similarity in peak positions and intensity distributions give confidence in the quality of the refinement and agreement for rather fine-grained Death Valley and Salton Sea clays is

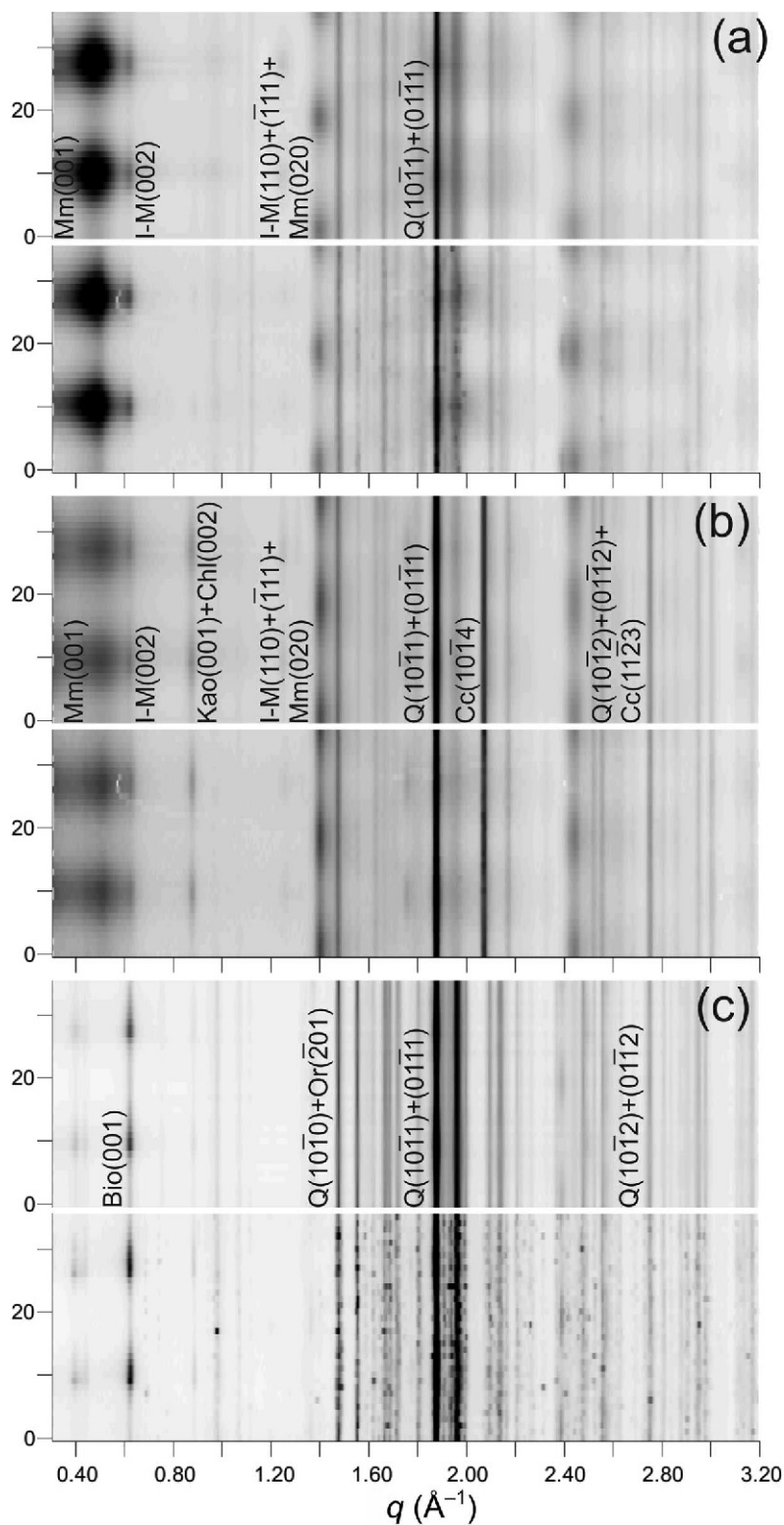


Figure 5. Unrolled diffraction images of: (a) Death Valley DV1; (b) Salton sea mud volcano SS2; and (c) Val Albigna glacial lake Brg1644 samples displaying intensity (gray shade) as a function of scattering vector magnitude  $q = 2\pi/d$  and azimuthal angle in diffraction image (corresponding to Figure 4), now made up of 36 diffraction patterns (numbered 0 through 35 on the left axis). For every image, the lowermost patterns show experimental intensities and uppermost patterns are the corresponding Rietveld refinement. For mineral abbreviations see Table 1.

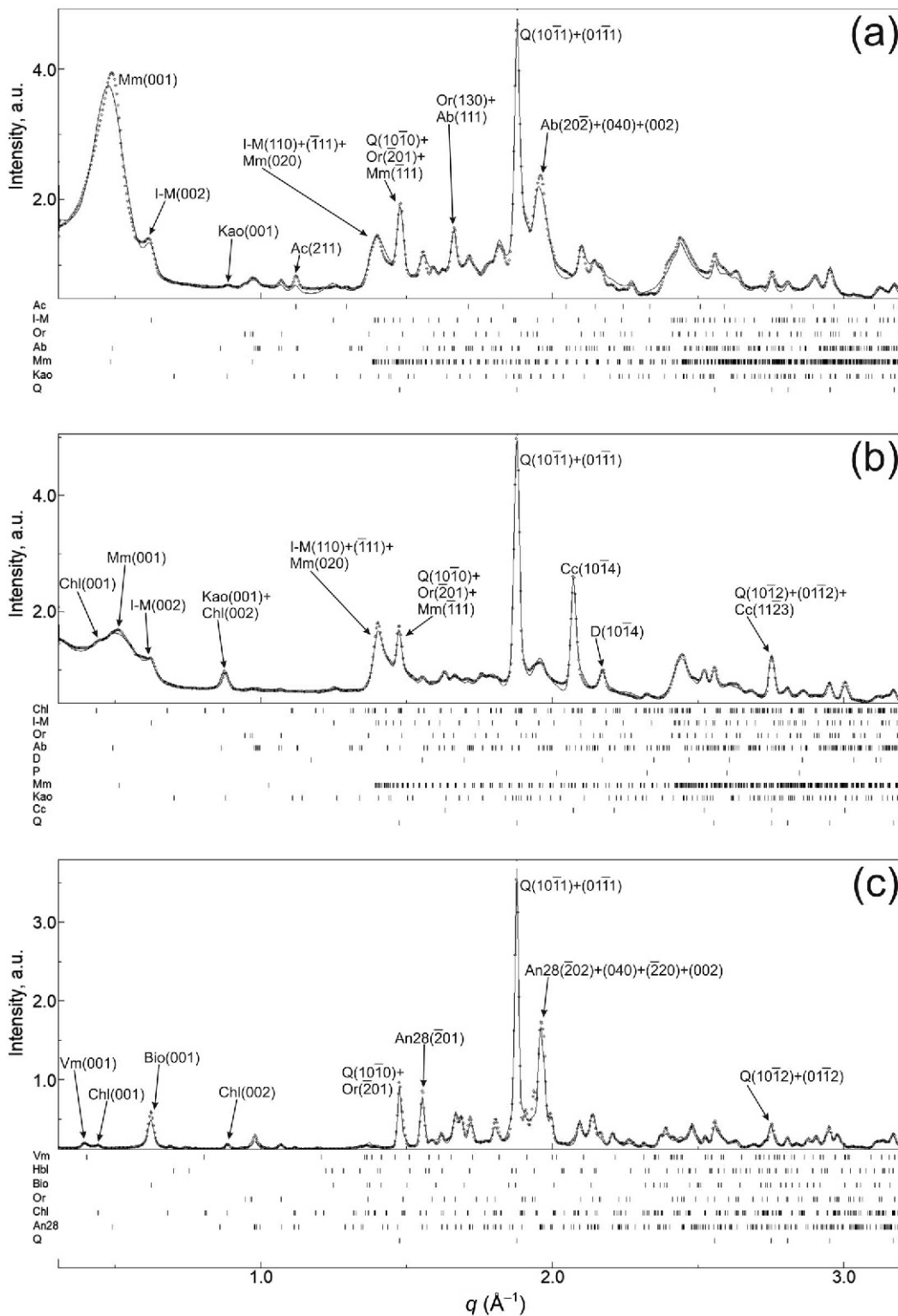


Figure 6. Average diffraction pattern for diffraction images (*cf.* Figures 4, 5) of: (a) Death Valley DV1; (b) Salton Sea mud volcano SS2; and (c) Val Albigna glacial lake Brg1644 samples with linear intensities plotted as a function of  $q = 2\pi/d$ . Dots are measured intensities and the solid line is Rietveld refinement. Diffraction-peak positions of minerals are shown by ticks (bottom). Multiple diffraction peaks of Mm (montmorillonite) are due to an applied stacking disorder model. Some diffraction peaks are labeled. For mineral abbreviations see Table 1.

excellent (Figure 5). In the case of Val Albigna, the model was not able to refine the spotty reflections from individual quartz and feldspar crystallites but provided a satisfactory fit for textures of phyllosilicates.

## RESULTS

The microstructures of all three samples are complex, as easily seen in SEM backscatter images (Figure 2). Within clusters of angular fragments, mainly quartz and feldspar, grains of phyllosilicates are observed. Some larger platelets, of illite-muscovite, are obviously oriented and define the bedding plane, indicated on the figures with white lines.

In the Death Valley clay (Figure 2a), a wide range of grain sizes is found. Large quartz fragments are  $\sim 10\ \mu\text{m}$  in diameter, illite-mica platelets have lengths of 10–20  $\mu\text{m}$ . In addition, a fine-grained matrix composed of montmorillonite and kaolinite is also present. Debye rings of quartz and feldspars in DV1 (Figure 4a) show occasional spots, characteristic of scattering by larger grains.

For the Salton Sea sample (Figure 2b), grain size is intermediate with granular quartz, feldspar, and calcite 5–10  $\mu\text{m}$  long, detrital illite-mica 10–20  $\mu\text{m}$  long, and fine-grained montmorillonite and kaolinite 1–5  $\mu\text{m}$  long. Fine montmorillonite is also layered but the alignment is less regular than for coarser illite-mica.

The simplest microstructure is observed in Val Albigna clay with oriented phyllosilicates in a granular matrix, with no secondary clay minerals (Figure 2c). This clay, when dried, loses its coherency, contrary to the other two. Mica platelets are  $\sim 1\ \mu\text{m}$  thick and 100  $\mu\text{m}$  wide, quartz and feldspar range from 10 to 100  $\mu\text{m}$  in width. The large grain size of quartz and feldspar produces a spotty diffraction image (Figure 4c).

EDS analyses of Death Valley and Salton Sea clay, averaging over a large surface area (1 mm  $\times$  1 mm),

indicate that Si is the dominant component, followed by Fe and Al (Figure 3). Death Valley clay has a significant amount of Mg ( $\sim 11\ \text{wt.}\%$ ) and K ( $\sim 10\ \text{wt.}\%$ ). Salton Sea clay is enriched in calcium ( $\sim 12\%$ ) and contains halite ( $\sim 3\%$  Cl, Figure 3b). The differences in chemical composition reflect the variations of the host rocks in the vicinity.

The Rietveld refinement provides volume fractions of constituent minerals (Table 1). Phyllosilicates make up about half of the volume for Death Valley and Salton Sea clay, while they are a small fraction in Val Albigna clay. The mineral composition reveals considerable diagenetic activity with growth of montmorillonite and kaolinite in the Death Valley and Salton Sea samples. These components are missing from Val Albigna clay, the composition of which reflects the composition of the granodioritic host rock in the valley.

The focus of the present study was the preferred orientation in surface clays represented as (001) pole figures (Figure 7) and a summary of quantitative data (Table 2).

The ODFs of montmorillonite and illite-mica in DV1 are sharp. Their minimum values (Table 2) indicate that only 17 vol.% of montmorillonite and 11 vol.% of illite-mica grains are randomly oriented (ODF minimum), while the ODF maximum of montmorillonite is 5.7 m.r.d. and of illite-mica 6.0 m.r.d., expressed in (001) pole figure maxima 3.1 m.r.d. and 4.0 m.r.d., respectively. (001) lattice planes are aligned preferentially in the bedding plane. In addition, a small fraction ( $\sim 0.01$ ) of kaolinite is present with a refined (001) lattice spacing of 7.09 Å. This diffraction peak demonstrates strong intensity variations along the Debye rings (Figures 4a, 5a), consistent with the preferred orientation of (001) poles normal to the bedding plane. Indeed, the kaolinite ODF shows the largest maximum and lowest minimum values (Table 2), but the (001) pole figure is somewhat distorted (Figure 7a), deviating from the

Table 1. Volume fractions of component minerals with the same abbreviations as used in the figures and figure captions.

Mineral	Abbreviation	Death Valley DV1	Salton Sea SS2	Val Albigna Brg1644
Montmorillonite	Mm	0.211	0.253	
Illite-mica	I-M	0.325	0.199	
Biotite	Bio			0.089
Chlorite	Chl		0.036	0.022
Kaolinite	Kao	0.010	0.076	
Vermiculite	Vm			0.003
Quartz	Q	0.107	0.167	0.212
Calcite	Cc		0.112	
Dolomite	D		0.023	
Plagioclase	Ab/An28	0.184	0.056	0.436
Orthoclase	Or	0.146	0.076	0.229
Pyrite	P		0.002	
Hornblende	Hbl			0.009
Analcime	Ac	0.017		



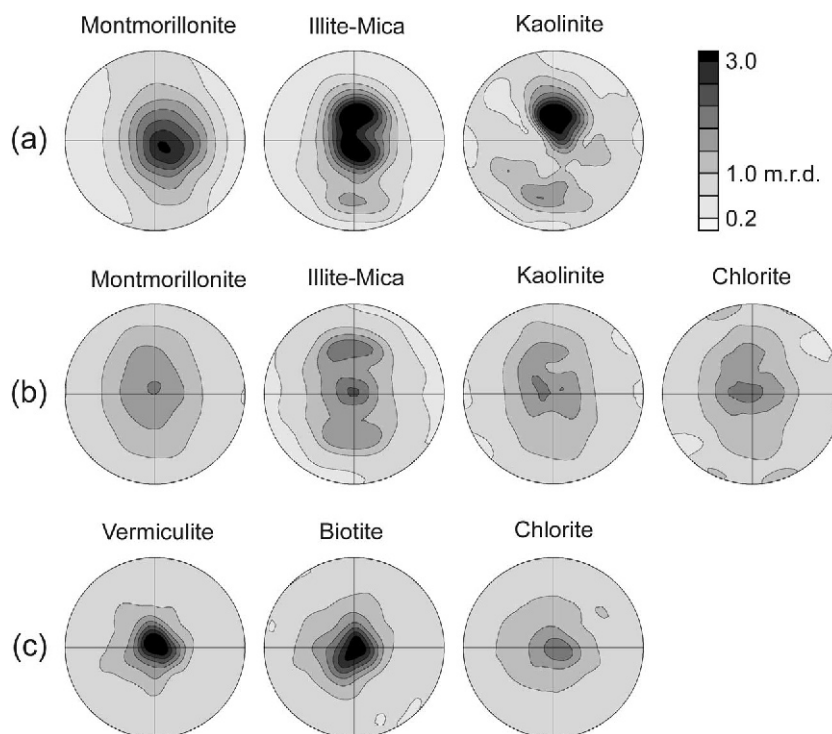


Figure 7. (001) Pole figures of phyllosilicates for: (a) Death Valley DV1; (b) Salton Sea mud volcano SS2; and (c) Val Albigna glacial lake Brg1644 samples. The linear-scale contours are given in multiples of a random distribution (m.r.d.). Equal area projection on the bedding plane.

orientation in the bedding plane. This may be caused partially by lower reliability because of the small volume fraction, because the texture strength is strongly affected by local background variations, and peak overlaps with the disordered montmorillonite. Quartz,

Table 2. Preferred orientation characterization of phyllosilicates with ODF maximum and minimum values and (001) pole figure maximum and minimum (in multiples of a random distribution).

	ODF max	ODF min	(001) max	(001) min
Death Valley DV1				
Montmorillonite	4.73	0.17	3.12	0.37
Illite-muscovite	5.95	0.11	4.03	0.27
Kaolinite	19.27	0.02	4.16	0.39
Salton Sea SS2				
Montmorillonite	2.14	0.50	1.85	0.59
Illite-muscovite	2.95	0.28	2.33	0.47
Kaolinite	2.88	0.32	1.90	0.55
Chlorite	3.43	0.09	2.05	0.51
Val Albigna Brg1644				
Biotite	5.22	0.31	3.45	0.58
Chlorite	2.56	0.59	2.15	0.80
Vermiculite	4.41	0.55	3.74	0.72

feldspars, and analcime appear to be randomly oriented.

To refine diffraction images of Salton Sea mud volcano sample SS2, ten minerals were considered (Table 1). Of those, montmorillonite, illite-mica, kaolinite, and chlorite were considered for texture analysis. Overall, preferred orientations of phyllosilicates were weaker than in Death Valley clay. ODF maxima are 2.1 m.r.d. for montmorillonite, 3.0 m.r.d. for illite-mica, and 2.9 m.r.d. for kaolinite (Table 2). The ODF minima are relatively high: 30–50 vol.% of illite-mica, kaolinite, and montmorillonite crystallites are randomly oriented as indicated by corresponding minimum ODF values (Table 2). Maximum values on (001) pole figures are  $\sim 2$  m.r.d., all with a fairly symmetrical maximum perpendicular to the bedding plane (Figure 7b). Compared with montmorillonite from Death Valley clay with a (001) diffraction peak position at  $d \approx 12.92$  Å, the position for Salton Sea mud volcano clay is at  $d \approx 12.22$  Å. These interlayer distances correspond to montmorillonites with a single water layer between clay layers in their crystal structure (e.g. Mazo *et al.*, 2008; Ebrahimi *et al.*, 2012); although, due to large disorder-related peak broadening, Salton Sea clay may contain partially dehydrated montmorillonite.

For Val Albigna clay, biotite, chlorite, and vermiculite display textures with very regular (001) maxima perpendicular to bedding (Figure 7c). Biotite and vermiculite which are present in minor amounts ((001)

lattice spacing is  $\sim 15.59 \text{ \AA}$ ) have ODF maxima of 5.2 and 4.4 m.r.d. respectively; for chlorite, the maximum is weaker (2.6 m.r.d.). All three phyllosilicates occur as fairly large platy particles. Montmorillonite and kaolinite are absent. Consequently, compared to Death Valley and Salton Sea, diffraction at very low angles (Figure 4 a,b) is also absent, indicating that it is indeed attributed to small-angle scattering on nanocrystalline montmorillonite.

All (001) pole figures show a maximum perpendicular to the bedding plane (Figure 7) but the strength of this maximum varies for different samples as well as different clay minerals. The girdle distribution for Death Valley and Salton Sea clay may be an artifact of incomplete pole figure coverage ( $-45^\circ$  to  $45^\circ$ ) compared with full coverage for Val Albigna ( $-90^\circ$  to  $75^\circ$ ) and sample heterogeneities, keeping in mind that information was extracted from small volumes ( $\sim 10 \text{ mm}^3$ ).

## DISCUSSION

The present report shows that three clay samples which formed in very different aqueous, non-marine, surface environments display significant preferred orientation of phyllosilicates. This is the first study documenting and quantifying alignment in such samples. All mineral components for which preferred orientation could be documented are phyllosilicates with a platy morphology parallel to the (001) crystal planes producing a close relation between crystal-preferred orientation (CPO) and shape-preferred orientation (SPO).

Death Valley clay displays the strongest alignment and the Mesquite Flat occurrence probably formed in a lake-like environment, most likely during a period of significant precipitation. A systematic investigation of clays in ancient desert lake/pool/stream environments would be illuminating. This obviously does not imply that all surface clays display orientation patterns. Specific conditions are required such as water pools with suspended phyllosilicates and minimal turbulence.

In Salton Sea mud volcanoes a high clay:liquid ratio with turbulent eruptions was found (Figure 1b), followed by slow settling and solidification. Of the three samples, the Salton Sea clay displayed the weakest preferred orientation. High preferred orientation develops during sedimentation in stable environments and is local. The high temperatures of the extruding mud favored alterations to clay minerals such as montmorillonite and kaolinite. In Death Valley and Salton Sea, clay phyllosilicates constitute about half of the volume.

The simplest evolution is that of the Val Albigna clay in an Arctic environment with glacial erosion of granodiorite and deposition in streams near the foot of the glacier and no precipitation of authigenic clays such as montmorillonite, though some biotite is altered to vermiculite (e.g. Acker and Bricker, 1992) but keeping the original morphology. Biotite and chlorite fragments

align in ponds. Significant alignment of crystallites is also observed here, even though phyllosilicates make up only a minor fraction ( $\sim 11 \text{ vol.}\%$ ).

How do these sedimentary surface clays compare with other phyllosilicate-bearing rocks, such as shales, slates, schists, gneisses, and serpentinites? Much attention has been paid to such rocks because phyllosilicate alignment is a major cause of seismic anisotropy in the crust. Some phyllosilicate-bearing rocks such as slates (e.g. Haerinck *et al.*, 2015) and schists (e.g. Wenk *et al.*, 2010) display very strong preferred orientation attained during recrystallization under stress. Others, such as fault gouge, generally show fairly random orientation patterns because of simple shear rotations of platelets (e.g. Buatier *et al.*, 2012; Janssen *et al.*, 2012, 2014), or only very local alignment (e.g. Janssen *et al.*, 2016).

Most attention has been dedicated to preferred orientation and anisotropy of shales, mainly because of the significance for hydrocarbon exploration (e.g. Johnston and Christensen, 1995). Some qualitative studies of the clay fabric used electron microscopy (e.g. O'Brien, 1970; Moon and Hurst, 1984). Later, the alignment of phyllosilicate crystallites was quantified with X-ray diffraction methods. The strength of preferred orientation in shales has been attributed to the phyllosilicate content (e.g. Curtis *et al.*, 1980), quartz grain size (e.g. Blatt and Schulz, 1976), and processes of mechanical compaction (e.g. Gipson, 1966) and diagenetic recrystallization (e.g. Ho *et al.*, 1999; Aplin *et al.*, 2006; Day-Stirrat *et al.*, 2008).

How do oceanic shales compare with surface water clays? A comparison of composition and phyllosilicate alignment of some natural shales displays a wide range of fabric strengths (3–10 m.r.d. in (001) pole figures) (Table 3) compared with somewhat lower strengths (1.9–4.2 m.r.d.) for the three surface clays investigated in this study (Table 2). The greatest strengths ( $\sim 10 \text{ m.r.d.}$ ) were reported for old compacted shales such as Carboniferous mudrock from Yorkshire (Curtis *et al.*, 1980) and Cambrian shale from Silver Hill, Montana (Wenk *et al.*, 2007). These are quite exceptional and most shales have strengths of 4–5 m.r.d.

Experimentally, the alignment of phyllosilicates is well known to increase with compaction and phyllosilicate content (e.g. Voltolini *et al.*, 2009). At 50 MPa axial compaction, texture strength is 7–8 m.r.d. for 100% illite and 3 m.r.d. for a 50% illite-50% quartz mixture. Such experiments are normally carried out, however, on homogeneous samples and ideal conditions that do not appear to apply to most natural shale conditions with many phases and significant local heterogeneity. Yet the compacted illite-quartz mixture has a similar texture strength to those of Death Valley and Val Albigna surface clays. Thus, mechanical compaction is not required to produce a high degree of preferred orientation, and the alignment of phyllosilicate platelets depends on many factors that vary for each

Table 3. Compilation of phyllosilicate and quartz (and calcite) content (in volume fractions) and preferred orientation (maximum pole density on (001) pole figures of phyllosilicates in m.r.d.) in several shales. Samples studied with similar methods as in this report are emphasized. They are listed in alphabetical order of authors.

Locality	Clay	Quartz Calcite	(001) max	Reference
Barnett clay, Texas, USA	0.5	0.4	6	Allan <i>et al.</i> (2016)
Yorkshire, UK	0.15–0.30		7–10	Curtis <i>et al.</i> (1980)
Posidonia, Hils syncline, Germany	0.3	0.15/0.4	4–5	Kanitpanyacharoen <i>et al.</i> (2012)
Qusaiba, South Africa	0.7	0.2	5	Kanitpanyacharoen <i>et al.</i> (2011)
Muderong, Australia	0.72	0.28	4–5	Kanitpanyacharoen <i>et al.</i> (2015)
Nigeria	0.8	0.15	3–5	Lonardelli <i>et al.</i> (2007)
Campine Basin, Belgium	0.75	0.1–0.2	4–7	Sintubin (1994)
Kimmeridge, UK	0.67	0.25	5	Vasin <i>et al.</i> (2013)
Mt. Terri, Switzerland	0.7	0.2/0.06	3–7	Wenk <i>et al.</i> (2008)
Silver Hill, Montana, USA	0.95	0.05	10	Wenk <i>et al.</i> (2007)

geological setting. Much of the phyllosilicate alignment of deeply buried mudrocks may occur at surface conditions in lake-like stable environments of lagoons, the continental shelf, and deep ocean settings.

Numerical simulations suggest that settling of isolated platy clay particles in an aqueous environment should lead to formation of significant preferred orientation because particles tend to reorient subnormal to the deposition direction and to be attracted to each other by torques of the opposite sign (*e.g.* Ardekani *et al.*, 2016). This can be compared with the procedure of settling clay powders in aqueous solutions to prepare oriented samples for X-ray powder diffraction to emphasize diffraction from basal planes that are diagnostic in terms of identification (*e.g.* Cody and Thompson, 1976; Moore and Reynolds, 1997, p. 214). Phyllosilicate platelets simply settle in a solution with particle shape and size causing some layering.

In natural conditions, such settling could be obstructed, or preferred orientation created by it could be, to some degree, altered by electrochemical, thermo-mechanical, and biogenic mechanisms (Bennett *et al.*, 1991). Flocculation of fine clay particles also leads to complex microstructures and may be responsible for the formation of weaker preferred orientation in settled phyllosilicates (*e.g.* O'Brien, 1971), though at least in some cases settling from flocculated suspensions may also create strong texture (*e.g.* Williamson, 1980).

In the glacial pool such as that at Val Albigna, settling of phyllosilicate particles occurs very locally with not much separation of phases. In Death Valley clay, the sedimentation occurred more homogeneously, probably in a large lake over considerable time, with significant alteration causing nanoscale formation of authigenic montmorillonite. The stable environment produced strong alignment. In Salton Sea mud, settling of crystals is constantly disturbed and old microstructural patterns are reworked, resulting in weaker alignment. Note, however, that these observations on three samples cannot be generalized to all surface mud

deposits. Clearly, not all surface clays display orientation patterns and specific conditions are required such as water pools with suspended phyllosilicates and minimal turbulence. The conditions have to be right; water with a high degree of phyllosilicate suspensions in an anoxic environment with not much organic material to avoid flocculation (*e.g.* Moon and Hurst, 1984).

## CONCLUSIONS

Mudstones in surface-lake environments can have strong preferred orientation of phyllosilicates, comparable to patterns observed in deep shales. This suggests that a significant portion of the alignment of phyllosilicates in deeply buried mudrocks may have occurred at an early stage, before modification by compaction and diagenesis. A systematic investigation of surface clays from various environments, including clays from oceanic basins, would be of interest in order to obtain a better understanding of the requirements for an early development of crystal preferred orientation. New experimental methods such as hard synchrotron X-ray diffraction have made available a quantitative approach to determine fabric patterns of complex polyphase mudrocks.

## ACKNOWLEDGMENTS

Diffraction experiments were conducted at the Advanced Light Source, Argonne National Laboratory, beamline 11-ID-C and the authors acknowledge the assistance offered by Yang Ren. SEM measurements were done at EPS-Berkeley and the University of Trento, Mesiano, Italy, and the authors are grateful for access and the help of Lorena Maines. Tim Teague helped with sample preparation. The authors are grateful to Mike Theiss (Instagram@ExtremeNature) for the picture of the Mesquite sand dunes. HRW acknowledges support from the National Science Foundation (Grant No. EAR-1343908) and the Department of Energy (Grant No. DE-FG02-05ER15637). Constructive reviews by Andreas Kronenberg and two anonymous reviewers, as well as the editors, were very helpful in improving the manuscript. Comments by Svetlana Vasina were also appreciated.

## REFERENCES

- Acker, J.G. and Bricker, O.P. (1992). The influence of PH on biotite dissolution and alteration kinetics at low temperature. *Geochimica and Cosmochimica Acta*, **56**, 3073–3092.
- Allan, A.M., Clark, A.C., Vanorio, T., Kanitpanyacharoen, W., and Wenk, H.-R. (2016) On the evolution of the elastic properties of organic-rich shale upon pyrolysis-induced thermal maturation. *Geophysics*, **81**, D271–D289.
- Almqvist, B.S.G. and Mainprice, D. (2017) Seismic properties and anisotropy of the continental crust: predictions based on mineral texture and rock microstructure. *Reviews of Geophysics*, **55**, 367–433.
- Antao, S.M., Hassan, I., Wang, J., Lee, P.L., and Toby, B.H. (2008) State-of-the-art high-resolution powder X-ray diffraction (HRPXRD) illustrated with Rietveld structure refinement of quartz, sodalite, tremolite, and meionite. *The Canadian Mineralogist*, **46**, 1501–1509.
- Aplin, A.C. and Larter, S.R. (2005) Fluid flow, pore pressure, wettability and leakage in mudstone cap rocks. Pp. 1–12 in: *Evaluating Fault and Cap Rock Seals*. American Association of Petroleum Geologists Hedberg Series No. 2 (P. Boulton and J. Kaldi, editors). American Association of Petroleum Geologists, Tulsa, Oklahoma, USA.
- Aplin, A.C., Matenaar, I.F., McCarty, D.K., and van der Pluijm, B.A. (2006) Influence of mechanical compaction and clay mineral diagenesis on the microfabric and pore-scale properties of deep-water Gulf of Mexico mudstones. *Clays and Clay Minerals*, **54**, 500–514.
- Ardekani, M.N., Costa, P., Breugem, W.P., and Brandt, L. (2016) Numerical study of the sedimentation of spheroidal particles. *International Journal of Multiphase Flow*, **87**, 16–34.
- Bennett, R.H., O'Brien, N.R., and Hulbert, H. (1991) Determinants of clay and shale microfabric signatures: Processes and mechanisms. Pp. 5–33 in: *Microstructure of Fine-Grained Sediments* (R.H. Bennett, W.R. Bryant, and M.H. Hulbert, editors). Springer Verlag, Berlin.
- Bish, D.L. and Von Dreele, R.B. (1989) Rietveld refinement of non-hydrogen atomic positions in kaolinite. *Clays and Clay Minerals*, **37**, 289–296.
- Blatt, H. and Schultz, D.J. (1976) Size distribution of quartz in mudrocks. *Sedimentology*, **23**, 857–866.
- Bossart, P. and Thury, M. (2007) Research in the Mont Terri Rock Laboratory: Quo vadis? *Physics and Chemistry of the Earth*, **32**, 19–31.
- Brigatti, M.F. and Davoli, P. (1990) Crystal-structure refinement of 1M plutonic biotites. *American Mineralogist*, **75**, 305–313.
- Buatier, M.D., Chauvet, A., Kanitpanyacharoen, W., Wenk, R., Ritz, J.F., and Jolivet, M. (2012) Origin and behavior of clay minerals in the Bogd fault gouge, Mongolia. *Journal of Structural Geology*, **34**, 77–90.
- Chadwick, R.A., Zweigel, P., Gregersen, U., Kirby, G.A., Holloway, S., and Johannessen, P.N. (2004) Geological reservoir characterization of a CO<sub>2</sub> storage site: The Utsira Sand, Sleipner, northern North Sea. *Energy*, **29**, 1371–1381.
- Cody, R.D. and Thompson, G.L. (1976) Quantitative X-ray powder diffraction analyses of clays using an orienting internal standard and pressed disks of bulk shale samples. *Clays and Clay Minerals*, **24**, 224–231.
- Curtis, C.D., Lipshie, S.R., Oertel, G., and Pearson, M.J. (1980) Clay orientation in some Upper Carboniferous mudrocks, its relationship to quartz content and some inferences about fissility, porosity and compactional history. *Sedimentology*, **27**, 333–339.
- Day-Stirrat, R.J., Aplin, A.C., Środoń, J., and van der Pluijm, B.A. (2008) Diagenetic reorientation of phyllosilicate minerals in Paleogene mudstones of the Podhale Basin, southern Poland. *Clays and Clay Minerals*, **56**, 100–111.
- De la Calle, C., Pezerat, H., and Gasperin, M. (1977) Problèmes d'ordre-désordre dans les vermiculites structure du mineral calcique hydraté a 2 couches. *Journal de Physique*, **38** (C7), 128–133.
- Downs, R.T., Hazen, R.M., and Finger, L.W. (1994) The high-pressure crystal chemistry of low albite and the origin of the pressure dependency of Al-Si ordering. *American Mineralogist*, **79**, 1042–1052.
- Dræge, A., Jakobsen, M., and Johansen, T.A. (2006) Rock physics modelling of shale diagenesis. *Petroleum Geoscience*, **12**, 49–57.
- Ebrahimi, D., Pellenq, R.J.-M., and Whittle, A.J. (2012) Nanoscale elastic properties of montmorillonite upon water adsorption. *Langmuir*, **28**, 16855–16863.
- Gatta, G.D., Nestola, F., and Ballaran, T.B. (2006) Elastic behavior, phase transition, and pressure induced structural evolution of analcime. *American Mineralogist*, **91**, 568–578.
- Gipson, M. (1966) A study of the relations with depth, porosity and clay-mineral orientation in Pennsylvanian Shales. *Journal of Sedimentary Petrology*, **36**, 888–903.
- Gournis, D., Lappas, A., Karakassides, M.A., Tobbens, D., and Moukarika, A. (2008) A neutron diffraction study of alkali cation migration in montmorillonites. *Physics and Chemistry of Minerals*, **35**, 49–58.
- Gualtieri, A.F. (2000) Accuracy of XRPD QPA using the combined Rietveld-RIR method. *Journal of Applied Crystallography*, **33**, 267–278.
- Haerincx, T., Wenk, H.-R., Debacker, T.N., and Sintubin, M. (2015) Preferred mineral orientation of a chloritoid-bearing slate in relation to its magnetic fabric. *Journal of Structural Geology*, **71**, 125–135.
- Helgeson, H.C. (1968) Geological and thermodynamic characteristics of the Salton Sea geothermal system. *American Journal of Science*, **266**, 129–166.
- Ho, N.-C., Peacor, D.R., and van der Pluijm, B.A. (1999) Preferred orientation of phyllosilicates in Gulf Coast mudstones and relation to the smectite–illite transition. *Clays and Clay Minerals*, **47**, 495–504.
- Hornby, B.E. (1998) Experimental laboratory determination of the dynamic elastic properties of wet, drained shales. *Journal of Geophysical Research*, **103**, 29945–29964.
- Janssen, C., Kanitpanyacharoen, W., Wenk, H.-R., Wirth, R., Morales, L., Rybacki, E., Kienast, M., and Dresen, G. (2012) Clay fabrics in SAFOD core samples. *Journal of Structural Geology*, **43**, 118–127.
- Janssen, C., Wirth, R., Wenk, H.-R., Morales, L., Naumann, R., Kienast, M., Song, S.R., and Dresen, G. (2014) Faulting processes in active faults – evidence from TCDP and SAFOD drill core samples. *Journal of Structural Geology*, **65**, 100–116.
- Janssen, C., Wenk, H.-R., Wirth, R., Morales, L., Kemnitz, H., Sulem, J., and Dresen, G. (2016) Microstructures and their implications for faulting processes – insights from DGLab core samples from the Gulf of Corinth. *Journal of Structural Geology*, **86**, 62–74.
- Johnston, J.E. and Christensen, N.I. (1995) Seismic anisotropy of shales. *Journal of Geophysical Research B*, **100**, 5991–6003.
- Kanitpanyacharoen, W., Wenk, H.-R., Kets, F., Lehr, B.C., and Wirth, R. (2011) Texture and anisotropy analysis of Qusaiba shales. *Geophysical Prospecting*, **59**, 536–556.
- Kanitpanyacharoen, W., Kets, F.B., Wenk, H.-R., and Wirth, R. (2012) Preferred orientation, microstructures and porosity analyses of Posidonia shales. *Clays and Clay Minerals*, **60**, 315–329.
- Kanitpanyacharoen, W., Vasin, R., Dewhurst, D., and Wenk, H.-R. (2015) Linking preferred orientations to elastic

- anisotropy in Muderong Shale, Australia. *Geophysics*, **80**, C1–C19.
- Lonardelli, I., Wenk, H.-R., and Ren, Y. (2007) Preferred orientation and elastic anisotropy in shales. *Geophysics*, **72**, D33–D40.
- Lutterotti, L., Voltolini, M., Wenk, H.-R., Bandyopadhyay, K., and Vanorio, T. (2010) Texture analysis of turbostratically disordered Ca-montmorillonite. *American Mineralogist*, **95**, 98–103.
- Lutterotti, L., Vasin, R., and Wenk, H.-R. (2014) Rietveld texture analysis from synchrotron diffraction images. I. Calibration and basic analysis. *Powder Diffraction*, **29**, 76–84.
- Mancini, F., Sillanpaa, R., Marshall, B., and Papunen, H. (1996) Magnesian hornblende from a metamorphosed ultramafic body in southwestern Finland: crystal chemistry and petrological implications. *The Canadian Mineralogist*, **34**, 835–844.
- Markgraf, S.A. and Reeder, R.J. (1985) High-temperature structure refinements of calcite and magnesite. *American Mineralogist*, **70**, 590–600.
- Matthies, S. (2002) 20 years WIMV, history, experience and contemporary developments. *Materials Science Forum*, **408–412**, 95–100.
- Matthies, S. and Vinel, G.W. (1982) On the reproduction of the orientation distribution function of textured samples from reduced pole figures using the concept of conditional ghost correction. *Physica Status Solidi*, **B 112**, K111–K114.
- Matthies, S. and Wenk, H.-R. (2009) Transformations for monoclinic crystal symmetry in texture analysis. *Journal of Applied Crystallography*, **42**, 564–571.
- Mazo, M.A., Manevitch, L.I., Gusarova, E.B., Shamaev, M.Y., Berlin, A.A., Balabaev, N.K., and Rutledge, G.C. (2008) Molecular dynamics simulation of thermomechanical properties of montmorillonite crystal. II. Hydrated montmorillonite crystal. *Journal of Physical Chemistry C*, **112**, 17056–17062.
- Moon, C.F. and Hurst, C.W. (1984) Fabric of muds and shales: an overview. Pp. 579–594 in: *Fine-Grained Sediments: Deep-Water Processes and Facies* (D.A.V. Stow and D.J.W. Piper, editors). Special Publication, **15**, Geological Society of London.
- Moore, D.M. and Reynolds Jr., R.C. (1997) *X-ray Diffraction and the Identification and Analysis of Clay Minerals*, 2nd edition. Oxford University Press, Oxford, UK, 378 pp.
- O'Brien, N.R. (1970) The fabric of shale – an electron microscope study. *Sedimentology*, **15**, 229–246.
- O'Brien, N.R. (1971) Fabric of kaolinite and illite floccules. *Clays and Clay Minerals*, **19**, 353–359.
- Phillips, M.W., Colville, A.A., and Ribbe, P.H. (1971) The crystal structures of two oligoclases: a comparison with low and high albite. *Zeitschrift für Kristallographie*, **133**, 43–65.
- Rieder, M., Crelling, J.C., Sustai, O., Drabek, M., Weiss, Z., and Klementova, M. (2007) Arsenic in iron disulfides in a brown coal from the North Bohemian Basin, Czech Republic. *International Journal of Coal Geology*, **71**, 115–121.
- Rietveld, H.M. (1969) A profile refinement method for nuclear and magnetic structures. *Journal of Applied Crystallography*, **2**, 65–71.
- Ross, N.L. and Reeder, R.J. (1992) High-pressure structural study of dolomite and ankerite. *American Mineralogist*, **77**, 412–421.
- Rudolph, M.L. and Manga, M. (2010) Mud volcano response to the 4 April 2010 El Mayor-Cucapah earthquake. *Journal of Geophysical Research: Solid Earth*, **115**, B12211, 1–14.
- Ruud, B.O., Jakobsen, M., and Johansen, T.A. (2003) Seismic properties of shales during compaction. *73rd SEG Meeting, Expanded abstracts, Dallas, Texas*, 1294–1297.
- Schneider, C.A., Rasband, W.S., and Eliceiri, K. W. (2012) NIH Image to ImageJ: 25 years of image analysis. *Nature Methods*, **9**(7), 671–675.
- Sintubin, M. (1994) Clay fabrics in relation to the burial history of shales. *Sedimentology*, **41**, 1161–1169.
- Sturz, A. (1989) Low-temperature hydrothermal alteration in near-surface sediments, Salton Sea geothermal area. *Journal of Geophysical Research: Solid Earth*, **94**, B4, 4015–4024.
- Tseng, H.-Y., Heanet, P.J., and Onstott, T.C. (1995) Characterization of lattice strain induced by neutron irradiation. *Physics and Chemistry of Minerals*, **22**, 399–405.
- Ufer, K., Roth, G., Kleeberg, R., Stanjek, H., Dohrmann, R., and Bergmann, J. (2004) Description of X-ray powder pattern of turbostratically disordered layer structures with a Rietveld compatible approach. *Zeitschrift für Kristallographie*, **219**, 519–527.
- Vasin, R., Wenk, H.-R., Kanitpanyacharoen, W., Matthies, S., and Wirth, R. (2013) Elastic anisotropy modeling of Kimmeridge Shale. *Journal of Geophysical Research*, **118**, 3931–3956.
- Voltolini, M., Wenk, H.-R., Mondol, N.H., Bjørlykke, K., and Jahren, J. (2009) Anisotropy of experimentally compressed kaolinite-illite-quartz mixtures. *Geophysics*, **74**, D13–D23.
- Wenk, H.-R., Matthies, S., Donovan, J., and Chateigner, D. (1998) BEARTEX: a Windows-based program system for quantitative texture analysis. *Journal of Applied Crystallography*, **31**, 262–269.
- Wenk, H.-R., Lonardelli, I., Franz, H., Nihei, K., and Nakagawa, S. (2007) Texture analysis and elastic anisotropy of illite clay. *Geophysics*, **72**, E69–75.
- Wenk, H.-R., Voltolini, M., Kern, H., Popp, H., and Mazurek, M. (2008) Anisotropy of Mont Terri Opalinus Clay. *The Leading Edge*, **27**, 742–748.
- Wenk, H.-R., Kanitpanyacharoen, W., and Voltolini, M. (2010) Preferred orientation of phyllosilicates: comparison of fault gouge, shale and schist. *Journal of Structural Geology*, **32**, 478–489.
- Wenk, H.-R., Lutterotti, L., Kaercher, P., Kanitpanyacharoen, W., Miyagi, L., and Vasin, R.N. (2014) Rietveld texture analysis from synchrotron diffraction images: II. Complex multiphase materials and diamond anvil cell experiments. *Powder Diffraction*, **29**, 172–192.
- Williamson, W.O. (1980) Experiments relevant to the genesis of clay mineral orientation in natural sediments. *Clay Minerals*, **15**, 95–97.
- Zanazzi, P.F., Comodi, P., Nazzareni, S., and Andreozzi, G.B. (2009) Thermal behaviour of chlorite: an in situ single-crystal and powder diffraction study. *European Journal of Mineralogy*, **21**, 581–589.

(Received 19 April 2017; revised 28 September 2017; Ms. 1175; AE: J. Kim)